PROPFAN NOISE PROPAGATION

Contract NAG-1-1078

Grant Monitor : F., Farassat

Final Report : September 1990 - August 1992

Principal Investigator : Albert R., George

Graduate Research Assistant : Ben Wel-C., Sim

Cornell University
Department of Mechanical & Aerospace Engineering
Ithaca, New York 14853-7501

Publications

1. Ben Wel-C., Sim and A. R., George, " A Study of Propfan Noise Propagation," AIAA Paper 93-0602, Presented at the AIAA 31st Aerospace Sciences Meeting, Reno, Nevada, January 1993.

2. Ben Wel-C., Sim and A. R., George, " A Survey of Propfan Noise Propagation at Cruise," To be presented at National Conference on Noise Control Engineering, Williamsburg, Virginia, May 1993.

3. Ben Wel-C, Sim, " Propfan Noise Propagation," M.S. thesis, Cornell University, 1993.

Note

The following final report is essentially the same as reference 1 above.

February 12, 1993

To : NASA Langley Research Center

From : Cornell University
Department of Mechanical & Aerospace Engineering

Subject : Propfan Noise Propagation
Final Report for Contract NAG-1-1078

---

1. Introduction

The unconventional supersonic tip speed of advanced propellers has led to uncertainties about Propfan's noise acceptability and compliance with Federal Aviation Noise Regulation (FAR 36). Overhead flight testing of the Propfan with SR-7L blade (figure 1) during 1989's Propfan Test Assessment (PTA) program[14] have shown unexpectedly high far-field sound pressure levels. This study here attempts to provide insights into the acoustics of a single-rotating propeller (SRP) with supersonic tip speed. At the same time, the role of the atmosphere in shaping the far-field noise characteristics is investigated.

A methodology for predicting noise due to supersonic blade tips based on geometrical acoustics is proposed. Our approach is to trace the emission of rays along a path determined by their local radiation cone. This is an extension of typical sonic boom analysis for a supersonic aircraft at level flight. Rays emitted in an inhomogeneous atmosphere undergo refraction according to Snell's law. Decreasing sound speed in a real atmosphere causes a ray to bend away from the ground which lengthens propagation distance and leads to additional sound attenuation. Amplitude variation along a given ray can be traced by employing the Blokhintzev energy invariant principle of geometrical acoustics in a motionless atmosphere. The principle can be expressed as a acoustic impedance (ρc) change factor, C_{imped} and a ray tube area (A) change factor, C_{area}. This analysis relies on the fact that disturbances are far away from the source such that the acoustic waves are locally plane, thereby justifying the use of geometrical acoustics and rays. Far-field acoustic pressures p' can be related to known near-field quantities by,

$$\frac{p'_{ff}}{p'_{nf}} = \sqrt{\frac{(\rho c)_{ff}}{(\rho c)_{nf}}} \sqrt{\frac{A_{nf}}{A_{ff}}} \qquad (1.1)$$

Analyses of various factors responsible for determining the far-field Propfan noise are documented. They can be essentially divided into two categories: Propagation and Atmospheric effects. Nonlinear wave steepening and geometrical decay are two of the well-known propagation effects. The calculations of these effects are carried out in the time domain due to their complexity. Atmospheric effects are dominated by energy depletion due to atmospheric absorption and turbulence scattering. Sound attenuation effects of absorption and scattering are examined in the frequency domain because of their dispersive nature. Examination of all these propagation and atmospheric effects are essential in the modeling of far-field Propfan noise.

Upon identifying the important phenomena affecting propagation noise, the next step is to assemble these factors together to determine their influence. This will allow us to study the physical aspects of sound propagation that leads to unacceptable Propfan noise annoyance. A FORTRAN program was developed at Cornell University which embodies all the relevant propagation and atmospheric effects to account for Propfan's far-field acoustics. This program analyses rays emitted from a helicoidal source path traced by supersonic helical speed blade tip. It is known that the amplitude disturbance in the vicinity of the of the tip envelope generates more sound than elsewhere along the blade. Earlier papers by Myers and Farassat[8] have demonstrated the presence of Mach envelopes that leads to formation of caustics. This nonlinear effect dominates the sound field. We use linear geometric acoustics to ascertain the existence of these nonlinear caustics in the far-field. The importance of caustics to Propfan noise generation is then studied.

2. Atmospheric and Propagation Effects

It is the aim of this section to examine the different factors that governs the acoustic strength after long distance of propagation in a ray tube. Effects of nonlinear wave steepening, atmospheric absorption and turbulence scattering are investigated. Discussion of attenuation due to geometrical spreading is delayed until the next section.

Nonlinear steepening

The study of acoustics is ordinarily concerned only with small amplitude disturbances. However, large amplitude pressure signals are known to be generated by the supersonic tip speed of the Propfan which are beyond the limits of linear acoustic formulations. In such cases, the nonlinear terms can lead to significant effects, because of long term accumulation of small nonlinear perturbations. The local velocity of a simple plane wave propagating in a homogeneous atmosphere (with ideal gas approximation) is given by,

$$\left[\frac{dx}{dt}\right] = c + \frac{\gamma+1}{2}\left\{\frac{p'}{\rho c}\right\} \tag{2.1}$$

Equation (2.1) has been derived for far-field plane waves with nonlinear steepening[4]. It demonstrates that the propagation velocity of each point on the wave is directly proportional to the local pressure amplitude. Pressure crests move faster than pressure troughs. Inequality of velocities at different points on the wave profile distorts the acoustic profile after long distance propagation. Compression points move forward and rarefaction points move in the opposite direction Eventually the waveform becomes such that the pressure signal is no longer single-valued. In actuality, discontinuities (shocks) are formed at locations that are multivalued. The strength and location of these discontinuities can be determined analytically by applying Whitham's[12] equal-area rule for weak shocks.

Our nonlinear steepening analysis is carried out based on the work of George and Plotkin[4]. Nonlinear calculations are conducted at incremental distances from the near-field. This method alters the wave profile accordingly by changing the arrival time of each point at every height interval. The new arrival time is calculated by adding to the initial time of arrival a Δt value corresponding to, (where r is the vertical distance from the mean propeller flight path and p is the ambient atmospheric pressure)

$$\Delta t = C_t\left\{\frac{p'}{p(r)}\right\}_{nf}\sqrt{r_{nf}} \tag{2.2}$$

where,

$$C_t = \frac{\gamma+1}{2\gamma c_0}\int^{r}\frac{p_{nf}}{p(r)}\left\{\frac{\rho(r)c_{nf}A_{nf}}{\rho_{nf}c(r)A(r)r_{nf}}\right\}^{\frac{1}{2}}\frac{M\,dr}{\sqrt{M^2-1}} \qquad (2.3)$$

Near-field thickness noise profiles calculated using the code DFP-ATP[1,2] Case 264 (cruise altitude: 9600 meters, tip speed: Mach 1.07) are shown in figure 2a. After employing the nonlinear wave steepening analysis the distorted waveform is shown in figure 2b based on ray tube areas calculated from cylindrical wave spreading. Notice that a narrow region of tripled-values region is formed as different portions of the wave propagates at different speed proportional to the local pressure amplitude. Peak pressure in figure 2b is 28 Pascal. Figure 2c indicates the far-field waveform after a shock has been fitted with in the multi-valued region. As a result the peak pressure decreases to 21.5 Pascal. Such a small change (2.2 dB) in pressure amplitude implies that the effect of nonlinear steepening is relatively minor. It is thus found that the tip pressure of the Propfan, though much higher than those generated by subsonic propellers, is not sufficient for the nonlinear effects to make important changes in the acoustic profile, except at caustics.

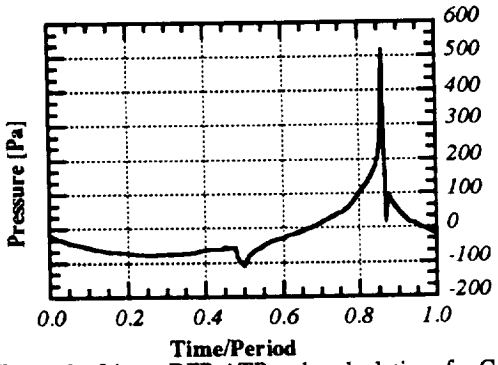

Figure 2a. Linear DFP-ATP code calculations for Case 264. The acoustic plot is for an observer situated 10 meters from the flight path. (Cruise altitude : 9600 meters).

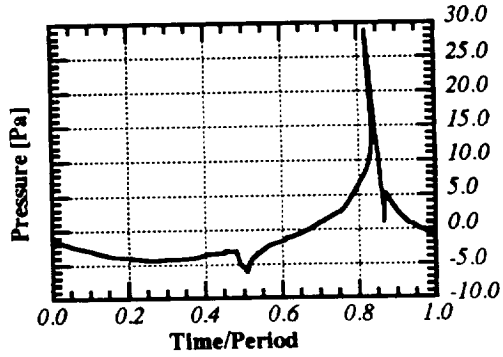

Figure 2b. Thickness noise profile of Case 264 for a ground observer after applying nonlinear analysis. Peak pressure is 28 Pa. Note the narrow triple-valued region at t/T=0.84.

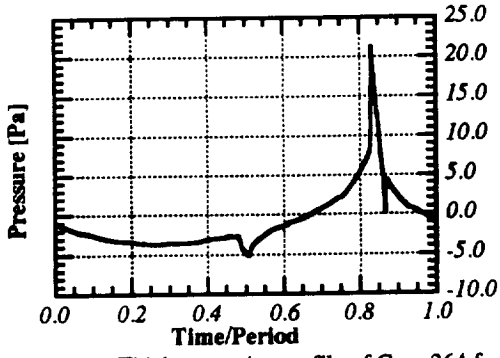

Figure 2c. Thickness noise profile of Case 264 for a ground observer after shock insertions by equal-area rule[12]. The peak pressure is now at 21.5 Pa.

Atmospheric absorption

It is known that atmospheric absorption is an important element in sound propagation over long distances. Energy dissipation due to sound absorption can be attributed by three basic mechanisms: *viscous* losses, *thermal conduction* losses and losses associated with *molecular exchanges of energy*. Processes by which losses due to molecular exchange of energy occurs are known as relaxation processes. Each of these processes is characterized by a relaxation time. There will be no appreciable dissipation if the relaxation time of a dissipating mechanism is long compared to the period of the acoustic cycle. In this section, the impact of all these three mechanisms will be studied to determine their effects within the audible range.

The combined effect of *viscous* and *thermal conduction* losses is known as *classical* relaxation. Viscous losses result whenever there is a relative motion between adjacent portions of the medium. For acoustic waves, the origin of viscous losses is primarily due to the compressions and expansions that accompany the wave transmission; while thermal conduction losses result from the conduction of heat between higher temperature condensations and lower temperature rarefactions. The analysis of classical absorption adopted from Pierce[10] assumes a linear acoustic formulation. The classical attenuation factor is typically represented by,

$$\left\{\frac{\alpha}{f^2}\right\}_{class} = \frac{1}{R_0}\int_0^{R_0} \frac{4\pi^2}{2\rho c}\left\{\frac{4}{3}\eta+(\gamma-1)\frac{k}{C_p}\right\} dr \qquad (2.4)$$

Absorption due to *molecular exchanges of energy* is essentially the result of the transfer of energy between different kinetic states of the molecule. The internal energy of gases in the atmosphere can be considered as a sum of the energy of individual molecules. Each molecule has a translational kinetic energy, rotational energy and vibrational energy. The latter two are negligible for a monatomic gas. If the gas is in equilibrium, the 'apparent' temperature associated with each kinetic state are the same. However, when a wave passes through a layer of the atmosphere, the molecules are initially excited translationally and are moved out of their equilibrium state. Energy is absorbed from the wave and redistributed among the three kinetic states in each molecule. There will be no absorption if the relaxation time for each internal state is much greater than the period of the acoustic cycle. On the other hand, if the relaxation time is very short compared to the period, the internal state will always be in equilibrium with the translational states and there will again be no absorption. Therefore molecular absorption will only take place for frequencies that are of order of the relaxation frequency (i.e., 1/relaxation time).

In the following analysis extracted from Pierce[10], only nitrogen and oxygen are considered since they are the main constituents in the middle atmosphere. Addition of water vapor into a mixture of gases can have considerable influence on absorption. Humidity in the atmosphere acts as a catalyst by decreasing the relaxation time of an absorption process and is accounted for by incoporating a humidity profile that was provided by PTA test program measurements into the analysis. For each type of molecule,

$$\alpha_{mole} = \frac{1}{\lambda}\frac{2\omega\tau_{mole}}{1+(\omega\tau_{mole})^2}[\alpha\lambda]_{mole} \quad , \quad [\alpha\lambda]_{mole} = \frac{\pi}{2}\frac{(\gamma-1)\left\{C_v\right\}_{mole}}{C_p} \qquad (2.5)$$

The relaxation time τ for each molecular type is given by,

$$\frac{p_{ref}}{p}\frac{1}{2\pi\,\tau_{O_2}} = 24+4.41\times10^{6}\,h\,\frac{0.05+100\,h}{0.391+100h} \tag{2.6}$$

$$\frac{p_{ref}}{p}\frac{1}{2\pi\,\tau_{N_2}} = \left\{\frac{T_{ref}}{T}\right\}^{\frac{1}{2}}\left\{9+3.5\times10^{4}\,h\,e^{-F}\right\} \tag{2.7}$$

where,

$$F = 6.142\left(\left\{\frac{T_{ref}}{T}\right\}^{\frac{1}{3}}-1\right) \tag{2.8}$$

$$h = \frac{10^{-2}\,(\text{Relative Humidity})p_{vp}\,T}{p} \tag{2.9}$$

Total absorption in the atmosphere is the cumulative sum of the equivalent classical absorption and effective molecular absorption associated with oxygen and nitrogen. Since the coefficients of each mechanism are rather small, it is assumed that all the relaxation processes act independently so as to allow a linear sum to be valid. Therefore, the total absorption coefficient is,

$$\alpha_{total} = f^2\left\{\frac{\alpha}{f^2}\right\}_{class} + \alpha_{O_2}(f)+\alpha_{N_2}(f) \tag{2.10}$$

Figure 3 shows the total absorption strength α_{total} in a real atmosphere calculated by integrating both classical and molecular absorption across the entire ray propagation distance. The attenuation coefficients are normalized by the Propfan's cruise altitude. Two conclusions can be drawn from here. Absorption in the audible frequency range is dominated by oxygen molecules. The overall effect tends to dissipate more energy from high frequency wave components. As a result, discontinuities and sharp spikes are removed in the far-field acoustic waveform.

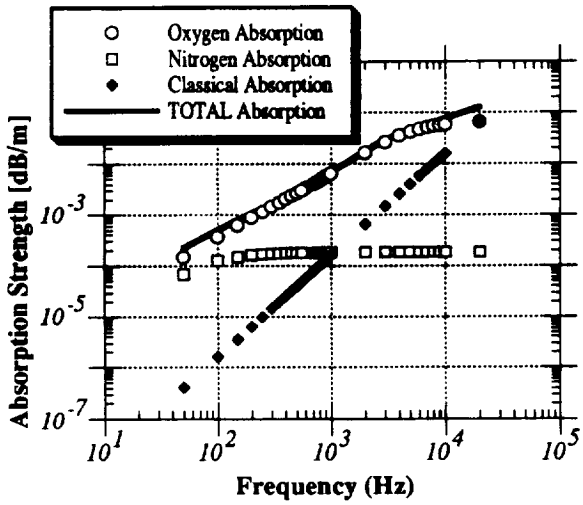

Figure 3. Attenuation due to classical and molecular absorption. Absorption strength is normalized by cruise altitude (9600m). Oxygen relaxation dominates between 20 Hz - 20 kHz range.

Turbulence scattering

Acoustic waves propagating in turbulent conditions have considerable fine-structures superposed on the basic far-field signal[14]. There is a variability in peak overpressures primarily associated with particular positive and negative spikes. Rise times are clearly longer than the assumed zero thickness jump. They are also longer than rise time expected from viscous or molecular absorption calculations. These phenomena are associated with turbulence in the atmospheric boundary layer particularly between sea-level and 1000 meters. This form of turbulence distortion is due to scattering and diffraction. Distortion is caused by random inhomogeneities in the atmosphere, which acts as secondary sources emitting scattered waves. These scattered waves appear as perturbations at or behind the original wave. As a result, scattered waves remove energy from the initial incident wave. The conditions required for this distortion to be evident is beyond the capability of geometrical acoustics. Instead, a separate theory has been developed by George and Plotkin[3] to account for scattering in isotropic turbulence.

The scattering analysis is modeled as a perturbation scheme with expansion parameter ε. Acoustic intensity of the wave after first order scattering I_1 (Born approximation) by isotropic turbulence can be modeled as a ratio of the initial intensity I_0 by,

$$s_{turb}(f) = \frac{I_1}{I_0} = e^{-\varepsilon^2 L_0 k_{wave}^2} \qquad (2.12)$$

where ε^2 is the turbulence intensity usually varying between 10^{-5} to 10^{-7}. L_0 is the macroscale length of the turbulence. The ratio of I_1 to I_0 is known as the first order scattering strength $s_{turb}(f)$. According to the scattering strength s_{turb} plotted in figure 4 for waves propagating in the atmospheric boundary layer, high frequencies are scattered more severely than low frequencies. The amount of energy scattered in each frequency increases with turbulence intensity. Comparing figure 4 with the absorption strength (figure 3), attenuation due to scattering within the atmospheric boundary layer is less significant than that due to absorption across the entire propagating space.

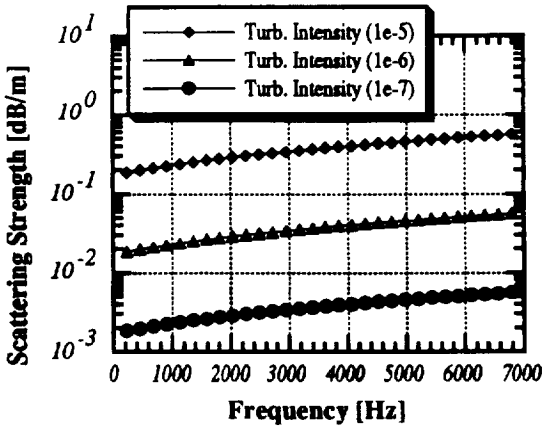

Figure 4. First-order scattering strength of isotropic turbulence. Scattering strength is represented by the value of $s_{turb}(f)$ which is for propagation in the atmospheric boundary layer thickness (1000 meters).

3. Computational Methods

In order to ease the analysis of Propfan noise propagation, a computer code based on geometrical acoustics was written. This FORTRAN code, named Linear Geometrical Acoustics (LGA), employs the concept of rays and ray tube areas to trace ray paths and amplitude variations. The program is designed to determine acoustic attenuations after long distance propagation in a horizontally stratified atmosphere with a constant sound speed gradient. The chief intention of this program is to investigate the effects of the Propfan's supersonic tip speed. Noise associated with supersonic motion has preferred directions of travel governed by the radiation cones at the source. (Radiation cones are normal to Mach cones as explained below) In essence, LGA consist of three parts. LGATrac is the first sub- program that performs the task of ray tracing. The second sub-program LGAArea calculates the ray tube area along a given ray. Finally LGAPropg determines the far-field acoustics taking into account various atmospheric effects discussed previously.

LGATrac

The underlying scheme of LGA is based on attaching a radiation cone to every discrete source lying on a path traced by the blade tip (figure 5). A radiation cone is the locus of all acoustic rays emitted from a supersonic source. These rays are defined by the direction where the velocity vector has a Mach number component in the direction of the observer equals to 1. Therefore, a radiation cone is always normal to the Mach cone surface. The path traced by a moving blade tip is a helix that can be parametrically represented by,

$$x_H = \eta' \mathrm{Cos}\left(\frac{\omega z_H}{V}\right) \qquad y_H = \eta' \mathrm{Sin}\left(\frac{\omega z_H}{V}\right) \tag{3.1}$$

where z_H is the projection of the helix distance on the Z axis. Selected ray at a base cone azimuthal angle ϕ is traced by LGATrac from cruise to observer height. A series of transformations is applied to convert the coordinate space of each three dimension ray propagation problem into two dimensions. This is plausible because the atmosphere is assumed to be horizontally stratified.

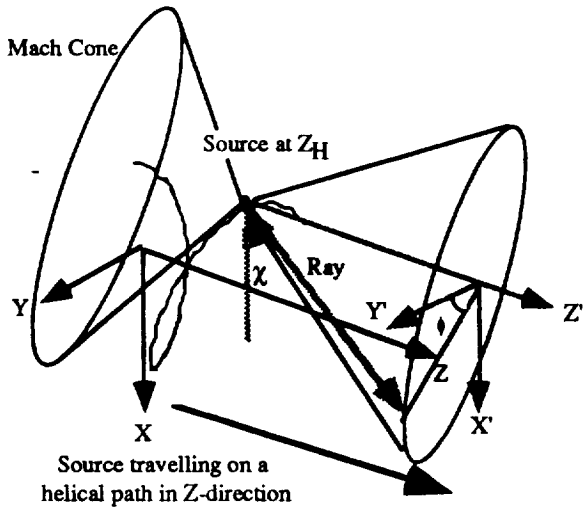

Figure 5. Schematic of LGA - a ray at z_H radiating from a supersonic source in helical motion with base cone angle ϕ. The ray will have an emission angle χ relative to X axis.

By geometrical acoustics, the problem can be reduced to a set of equations governed by z_H, ϕ and R. The location of a ray at R meters away vertically from the flight path can be represented by,

$$y'_{ffr} = y_H - \zeta \, Sin(\alpha-\lambda) \qquad z'_{ffr} = z_H + \zeta \, Cos(\alpha-\lambda) \tag{3.2}$$

where,

$$\zeta = \int_0^R \frac{\left(\frac{c(r)}{c_0}\right) Sin\chi \, dr}{\sqrt{1-\left(\frac{c(r)}{c_0} Sin\chi\right)^2}} \tag{3.3}$$

$$\alpha = Tan^{-1}\left(\frac{-\omega x_H}{V}\right) \quad , \quad \lambda = Tan^{-1}\left(\frac{Sin\phi}{Tan\Theta_0}\right) \tag{3.4 \& 3.5}$$

$$\chi = Cos^{-1}\left(Cos\Theta_0 \, Cos\phi\right) + \eta - \frac{\pi}{2} \tag{3.6}$$

$$\Theta_0 = Sin^{-1}\left(\frac{c_0}{\sqrt{V^2+\omega^2\eta'^2}}\right) \tag{3.7}$$

$$\eta = Tan^{-1}\left(-\frac{V}{\omega y_H}\right) \tag{3.8}$$

LGAArea

LGAArea calculates the ray tube area variations along a given ray. The ray tube area is an important quantity because it controls the degree of attenuation due to geometrical spreading of the wavefronts (geometrical decay). It is not possible to obtain a closed form area expression for rays emitted from a helix. Instead, a numerical approach is employed based on Hayes et al[6]. Ray tube area is calculated by using three rays originating in close proximity (figure 6). A reference ray [ray 1] at (z_H,ϕ) is chosen with two other neighboring rays [ray 2] and [ray 3] at $(z_H+\Delta z,\phi)$ and $(z_H,\phi+\Delta\phi)$ respectively. As these rays propagate into the far-field, a triangular area A_{tri} formed by these rays in the horizontal plane can be calculated . The actual ray tube area A is evaluated by taking the projection of A_{tri} in a plane perpendicular to the reference ray. In order for A to be determined, the far-field y and z coordinates of each ray must be calculated by LGATrac. Using Heron's formula,

$$A_{tri} = \sqrt{(s-a)(s-b)(s-c)} \quad , \quad s = \frac{a+b+c}{2} \tag{3.9}$$

where,

$$a = \sqrt{(y_{ray1}-y_{ray2})^2+(z_{ray1}-z_{ray2})^2} \tag{3.10}$$

$$b = \sqrt{(y_{ray2}-y_{ray3})^2+(z_{ray2}-z_{ray3})^2} \tag{3.11}$$

$$c = \sqrt{(y_{ray3}-y_{ray1})^2+(z_{ray3}-z_{ray1})^2} \tag{3.12}$$

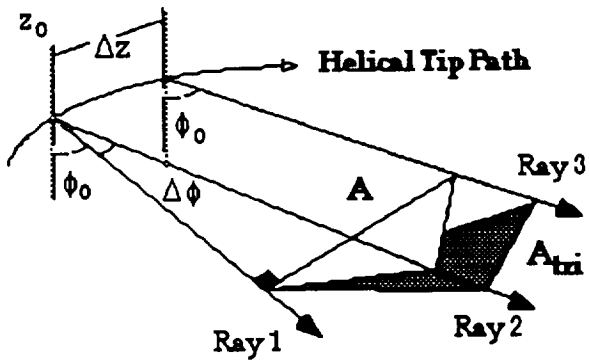

Figure 6. Formation of ray tube area A by three adjacent rays

To obtain the ray tube area A along the ray path, it is necessary to take the component of A_{tri} perpendicular to the reference ray by using equation (3.13).

$$A = A_{tri}\sqrt{1-\left(\frac{c_R}{c_0}\mathrm{Sin}(\chi)\right)^2} \tag{3.13}$$

LGAPropg

The final portion of the LGA program couples both the ray tracing theory and geometrical acoustics with the important atmospheric and propagation effects already discussed. The objective of this program is to predict the acoustic characteristics of Propfan cruise noise in the far-field, given the acoustic spectrum in the near-field. Near-field acoustics are obtained from the program DFP-ATP[1,2]. LGAPropg embodies the effects of geometrical decay (which is the product of C_{imped} and C_{area}), atmospheric absorption and turbulence scattering. Nonlinear effects have been left out because of their small influence on the acoustic amplitude and difficulty in introducing the effect into our computational model. A layer-by-layer technique would be necessary to determine the balance of nonlinear effects which introduce high frequency components versus atmospheric dissipations that reduce the energy of high frequencies.

Since nonlinear effects are neglected, implementation of LGAPropg is performed in the frequency domain across the entire propagation space as a whole. The far-field acoustics strength is calculated by modifying the Blokhintzev energy invariant principle. Instead of merely accounting for changes due to impedance and ray tube area, the effects of absorption and scattering are introduced in terms of frequency components as shown in equation (3.15). The attenuation strength for these atmospheric effects have been previously determined. L_{ray} corresponds to the total ray propagation distance to observer and L_{atm} is the distance the ray traveled within the atmospheric boundary layer, taking into account atmospheric refraction.

$$\frac{p'_{ff}[f]}{p'_{nf}[f]} = C_{imped}\, C_{area}\, C_{abs}[f]\, C_{turb}[f] \tag{3.14}$$

where,

$$C_{abs}[f] = 10^{\left\{\frac{-\alpha_{total}[f]\, L_{ray}}{20}\right\}}, \quad C_{turb}[f] = 10^{\left\{\frac{-s_{turb}[f]\, L_{atm}}{10}\right\}} \tag{3.15}$$

4. Results and Comparisons

The computational results of LGA are reported in this section. It is important to understand the various mechanisms at work affecting Propfan noise propagation. With the LGA program, these mechanisms can be carefully studied to determine their role in shaping far-field acoustics. In addition, the geometry of Propfan's noise carpet is presented along with some detailed discussion of the caustics that are present. An attempt to predict far-field Propfan noise is carried out at the end of this section. In all of the LGA runs, the flight parameters are fixed at the following values,

Cruise Altitude	= 9600 m
Cruise Mach Number	= 0.698
Angular Rotation	= 177.78 rad/sec
Blade Radius	= 1.372 m
Cruise Sound Speed	= 300 m/s
Ground Sound Speed	= 340 m/s

Noise carpet

Several interesting results were discovered. The first of them shows a distinct role of the helix path angle λ and η in setting a limitation on the ray emission angle χ. A smaller ray emission angle results in a shorter distance of propagation and hence a shorter time for propagation and atmospheric effects to dissipate energy. It was discovered that only the portion of the source helical motion with a local velocity directed towards the ground emits rays that will propagate to observers at lower altitudes with significant acoustical importance. The basis of this finding is entirely geometrical. A minimum emission angle χ_{min} can be determined from tip path geometry and Mach angle as follow,

$$\chi_{min} = \mathrm{Sin}^{-1}\left(\frac{1}{M_{tip}}\right) + \mathrm{Tan}^{-1}\left(\frac{V}{\omega\eta'}\right) - \frac{\pi}{2} \qquad (4.1)$$

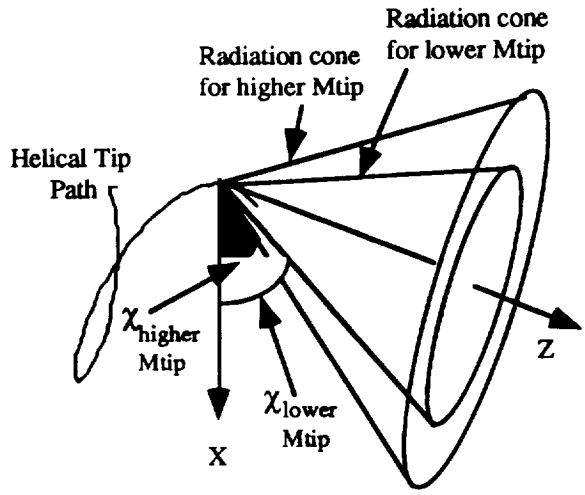

Figure 7. Variation of ray emission angle χ with tip Mach number. A lower tip Mach number has a smaller cone angle.

The minimum emission angle χ_{min} is 15.3° in our example. A ray emitting at χ_{min} experiences the shortest propagation distance and thus carries the loudest noise to the far-field. This ray also marks the first encounter of an observer with the Propfan's supersonic tip noise. Any other rays radiated will have a greater χ and longer propagation distance. A plausible way to reduce propagation noise is therefore to increase χ_{min} as much as possible by decreasing M_{tip}.

With the aid of LGA, a noise carpet can be drawn for the Propfan. A noise carpet is a ground acoustical footprint of all the rays emitted from the source path after one blade revolution. In order to better understand the various phenomenon contributing to the shape of the noise carpet, a brief account of how the acoustic waves radiates from a helicoidal supersonic source is presented here based on the work of reference 7 and 8. Figure 7a and 7b depicts the position of spherical sound waves after the propeller has attain one full revolution from two different perspectives. The result is the formation of a secondary envelope wavefront that represents a surface spiraling away from the flight path with increasing size in figure 7a. These secondary wavefronts represent a coalition of wavefronts radiating from the helical path. Small crescent-like cells (Mach envelopes) are observed in figure 7b. These cells are embedded within the secondary wavefront that appears to be advancing away from the flight path as the source moves along the helix path. At the end of each Mach envelope are points referred to as cusps, which are formed by the intersection of multiple signals. The illuminated region in figure 8b shows that the locus of these cusps can be traced by a hyperbolic surface[8]. Acoustic disturbances are expected to be louder inside these Mach envelopes and on the cusps than compared to disturbances in the shadow region due to many spherical wavefronts coalescing together. The difference between the cells and the cusps will be explained in greater detail.

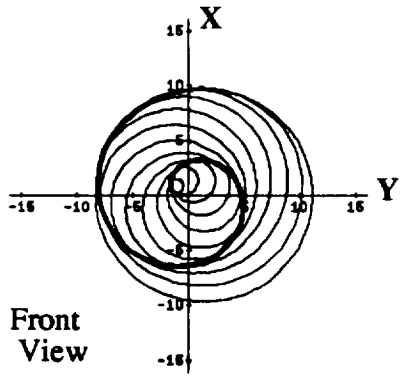

Figure 7a. Picture [Front View] of caustics formed by spherical signals originating from a helical source path.

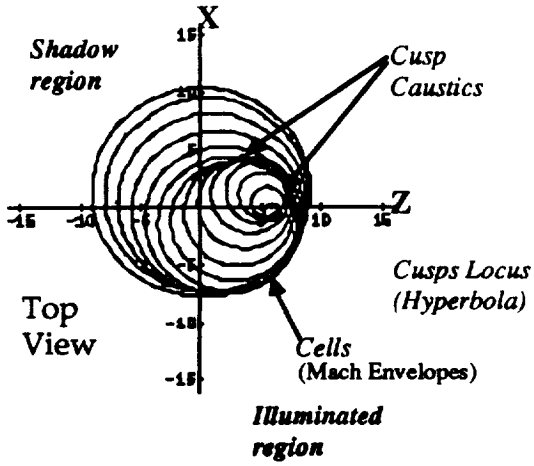

Figure 7b. Picture [Top View] of caustics wavefront generated by spherical signals originating from a helical source path. Note the formation of cusps and cells (Mach envelopes).

Figure 8 shows the noise carpet after the tip has undergone one full revolution with the base cone azimuthal angle ϕ for each ray subjected to values between -90° and +90°. The origin defines the location of the aircraft when the rays are emitted. From figure 8, the noise carpet is comprised of myriad parabolas that are formed by the intersection of radiation cones with the ground plane. The overall sound carpet is shaped like a fan with an uncomputed zone at the middle. This uncomputed zone embodies rays emitted with

base cone azimuthal angles ϕ beyond $\pm 90°$- which are omitted in our numerical calculations. The core of the carpet contains the most significant noise disturbance. Noise in the core is greater than in the outer region brought about by smaller distance of propagation. An outer limit can be clearly observed. This outer limit represents the atmospheric caustics-ground locus which marks the locations where the refracted rays become parallel to the ground plane due to atmospheric ray bending. No supersonic tip generated noise will be heard beyond this limit. An inner limit is also observed which defines the cusps caustics-ground locus. Points residing on this inner limit correspond to locations where cusps singularities occur. The cusps caustics-ground locus (inner limit) calculated by the LGA code is consistent with the hyperbolic cusp locus predicted by Myers and Farassat[8].

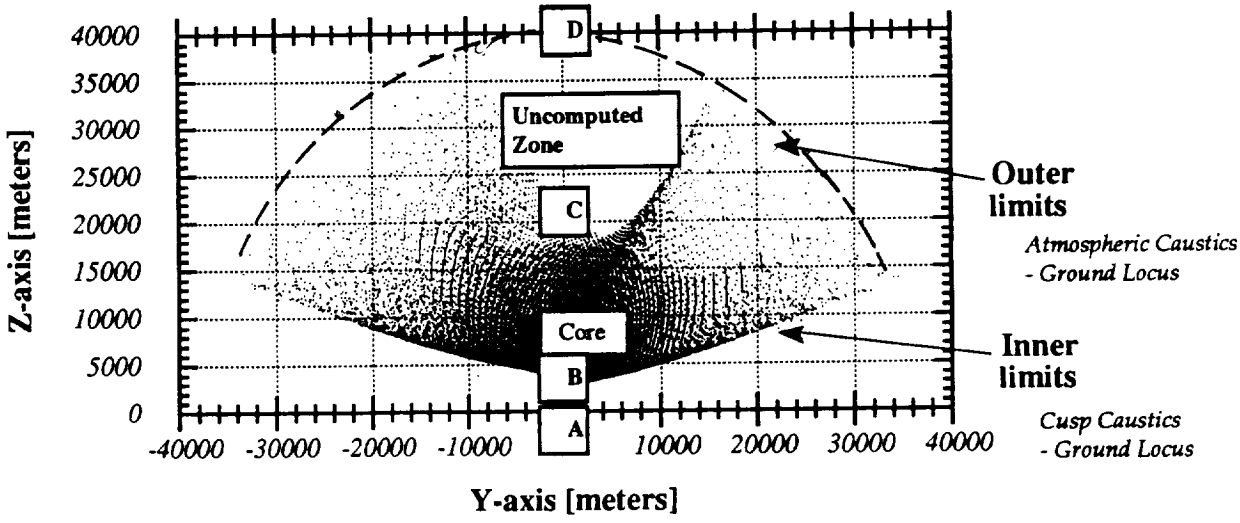

Figure 8. Noise carpet at sea-level for a Propfan cruising at 9600 meters.

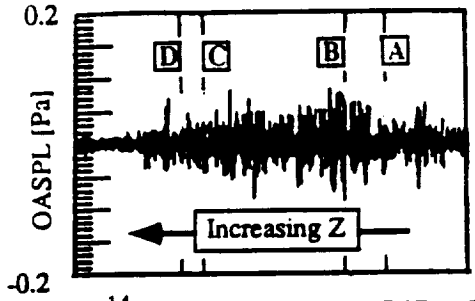

Figure 8a. PTA experiment[14] time history across line ABCD on Propfan's noise carpet.

Figure 8a shows the measured PTA[14] overall sound pressure level (OASPL) at different observer locations A, B, C and D along the Y=0 axis. Observer A is fixed at the origin while observer B is located on the inner limit line that traces the cusps locations on the ground. Observer at C is positioned at the edge between the uncomputed zone and the core. Finally, observer D is situated on the outer limit line which prescribes the atmospheric caustics-ground locus. The Propfan is stationed at 9600m above the origin.

As expected from the schematics of caustics wavefront (figure 7b), the OASPL has the highest level at observer B. Observer at A has a relatively low sound pressure level because there are no rays carrying the supersonic blade tip noise reaching the location. On the other hand, observer B experiences the full effect of the cusp caustics because it is

situated on the cusp caustics-ground locus. Observer C marks the beginning of the computational zone-of-silence. Noise at observer C is comparatively smaller than at B because the arriving rays have to propagate through a longer distance. The weakest overall sound pressure level can be found at location D. Even though observer D is residing on the atmospheric caustics-ground locus, the acoustic energy carried by the rays would have been attenuated drastically by atmospheric effects rendering the 7-12 dB increase due to atmospheric caustics[5] insignificant. For any other regions outside the area bounded by both the inner and outer limit, acoustic disturbance will not be due to the Propfan's supersonic tip speed.

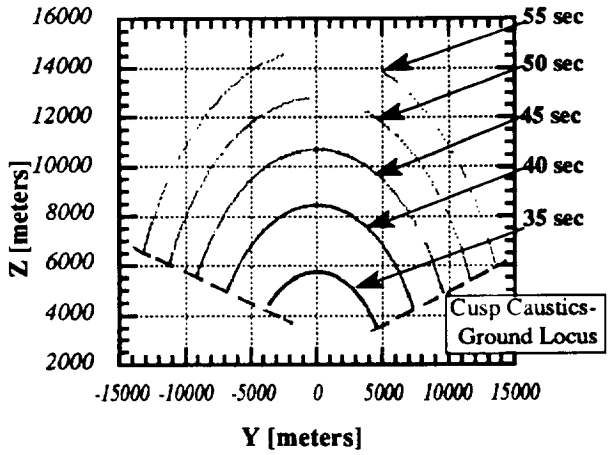

Figure 9. Ground traces of Propfan noise at different arrival times. These ground traces resembles the Mach envelopes in Myers and Farassat[8].

Ray tube area variations

It is observed that the entire sound carpet is comprised of a closely knitted array of ground traces. Figure 9 shows the ground traces evaluated at different times of arrival from 35 to 55 sec. Ground traces are collections of ray-ground intersection points at some instant of time. It can be observed in figure 9 that these ground traces arrange themselves in the form of an arc which "propagates" away from the origin along the ground plane. The formation of these arcs correspond to Mach envelopes observed in figure 7b. These ground traces may or may not carry rays that intersect each other on the ground simultaneously.

A detail investigation of the variation of the ray tube area across the sound carpet is conducted to determine the ray activities within the noise carpet. Figure 10 shows how the ray tube area changes along the Y-axis at fixed Z. A_{ref} is the reference ray tube area at 20 meters away from the source path. The arrival time of each ray is included to indicate the various moments at which the ray reaches the ground plane. It has already been illustrated (figure 9) that the rays arrive in the form of an arc which "radiates" along the ground plane towards the positive Z direction. Therefore an observer standing at the location Z=5000m will progressively experience the impact of rays as the arcs pass by. From figure 10, the very first arc arrives at Y = 0 meters after 34 seconds. The ray tube area plot indicates that there are two rays arriving at every Y location at the same time across the span of -6500 to 10000 meters. This result confirms the existence of caustics in the sound carpet due to the rotating geometry of the source distribution along the helical tip path described in the work of Lowson and Jupe[7]. The caustics within the sound carpet correspond to the cell caustics in figure 7b and are formed by two rays. At the end points along the arc, there are apparently more than two rays arriving at the same time. These end points correspond to locations prescribed by the inner limit and are therefore the cusp

caustics. It is not possible to state the exact number of rays arriving at any cusps by our numerical calculation because the point is singular. Moreover, the ray tube areas accompanying these rays ranges across a wide spectrum. It is likely that the acoustic strength at these cusps will be a great many times that of the acoustic amplitude for nearby points inside the carpet.

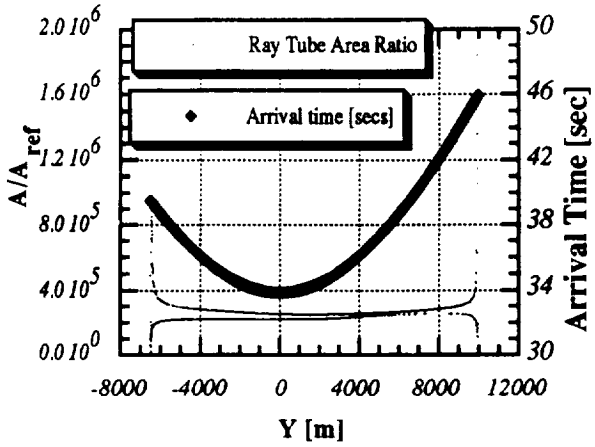

Figure 10. Variation of Ray tube area factor across Y-axis at Z=5000 meters. Arrival time of each ray is also illustrated.

Geometrical decay

Geometrical decay governs the acoustic energy depletion in a homogeneous atmosphere. Figure 11 illustrates the variation of acoustic impedance and ray tube area correction factor with distances along the propagating ray path which is not near a caustic. The ray tube area correction factors are shown for emission source at 3/4 blade revolution and with ray emitted at an angle $\phi = 0°$. The geometrical decay of the propagating wave amplitude is given by the product of the acoustic impedance C_{imped} and the ray tube area correction factor C_{area} at the same altitude. It can be seen that the decay is dominated by variations in the ray tube area. Acoustic impedance only begins to have a significant effect on geometrical spreading in the far-field. The amplitude decay is discovered to vary with $r^{-0.91}$. This factor falls between geometrical decay for spherical waves r^{-1} and cylindrical waves $r^{-0.5}$, which was the range predicted by Myers and Farassat[8].

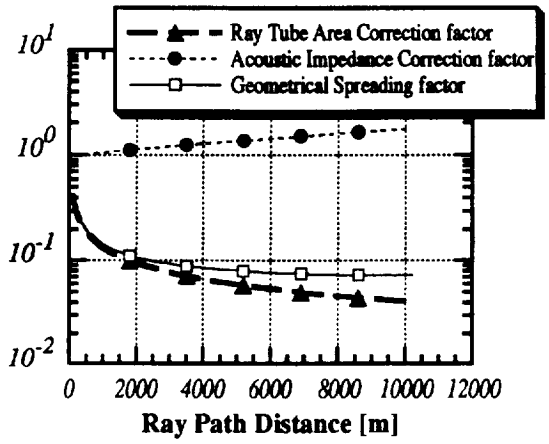

Figure 11. Variation of geometrical decay factor along a ray path. Ray is emitted from 3/4 blade revolution and ϕ=0°.

Sound attenuation

Next, a comparative investigation of the various sound attenuating effects is in order. Figure 12 illustrates the attenuation strength of both propagation and atmospheric effects with frequency for the case of a ray radiating from 3/4 period and an emission base cone azimuthal angle ϕ=0°. The strength of attenuation for each factor is expressed in terms of the decibel level after propagation from the cruise altitude to sea-level. Since the coefficients due to acoustic impedance C_{imped} and ray tube area C_{area} are derived from linear geometrical theory, they are constant over the entire frequency spectrum. The coefficients for sound absorption C_{abs} and turbulence scattering C_{turb} are, on the other hand, dispersive. These coefficients vary with frequency and has the tendency to attenuate more energy from the higher harmonics. However, the change in the turbulence scattering coefficient is so small that it can hardly be seen on the plot. The sound attenuation plot indicates that the ray tube area and atmospheric absorption are the predominant elements of propagation noise reduction. Most of the sound below 1000 Hz are dissipated by the action of expanding ray tube area. The decrease in sound level due to ray tube area expansion amounts to 61 dB. As the frequency increases beyond 1000 Hz, molecular absorption in the atmospheric begins to account for most of the sound loss. Attenuation coefficients for frequencies higher than 2000 Hz are not displayed because of the exceedingly large absorption coefficients.

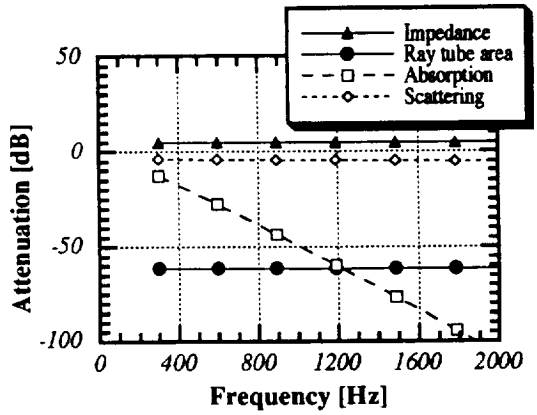

Figure 12. Sound attenuation at sea-level due to propagation and atmospheric effects for a ray emitted at cruise altitude, 3/4 period and ϕ=0°.

Far-field noise prediction

The final task of the LGA code is to offer a reasonable prediction of Propfan propagation noise with the important atmospheric effects taken into account. In the following comparisons, we try to establish what are the essential factors governing the far-field acoustic strength and the elements that should be considered to improve Propfan propagation noise prediction in the future. The Propfan sound carpet is now understood to consist of essentially only caustic points. Even though the theory of geometrical acoustics breaks down at caustics, it is still possible to estimate the noise level in the core as long as the observer is not on the Mach envelope-ground intersection locus where the points are singular. A simple approximate theory based on ray interference was implemented. Since each point within the core is made up of two arriving rays, it is appropriate to visualize the pressure amplitude at the point to be contributed by two sources situated on the helical tip path far away. Furthermore, the ray tube area of these rays emitted from each of these two sources were found to be closely similar. With the propagation distance of the two rays almost equal, we can therefore conclude that the two acoustic ray strength are correlated and nearly similar. The far-field acoustic pressure can therefore be

approximated by the linear sum of the individual pressure of these two sources. A second assumption added to post-LGA computations is the introduction of multiple blade effects. Since the full Propfan set up consist of 8 blades and far-field LGA computation only accounts for one single tip source, the acoustic power obtained from LGA are multiplied eight folds to obtain the total acoustic power. Interference effects are neglected. This procedure is valid for in phase signal arrivals.

Figure 13 shows the far-field LGA predictions compared with Lockheed's Propfan Test Assessment data[14] and NASA's Aircraft Noise Predicting program[13]. It was decided that only the first three harmonics of the Propfan's acoustic spectrum are useful because of two reasons. The first is the limited dynamic range of the PTA data collected. The second reason arises from the analysis of LGA which reveals insignificant amplitudes at higher harmonics due to tremendous dissipation by atmospheric effects. The general result shows that LGA provides an adequate mean of predicting far-field Propfan noise. Fundamental noise is predicted well at 58 dB. The second harmonic consistently shows more deviation from PTA data at 37 dB while the third harmonic register an insignificant noise amplitude of 18 dB. The reason for the large discrepancy at the second harmonic is not understood at the moment. A possible reason is that the limited dynamic range of the microphones used in PTA has also contaminated the values at the second harmonic. However, this has not be verified. The general trend of LGA predictions show a diminishing acoustic strength with increasing frequency. ANOPP predictions are commonly higher because turbulence scattering in the atmospheric boundary layer is not taken into consideration. Therefore, it is concluded that atmospheric turbulence scattering should be included for better far-field predictions in the future.

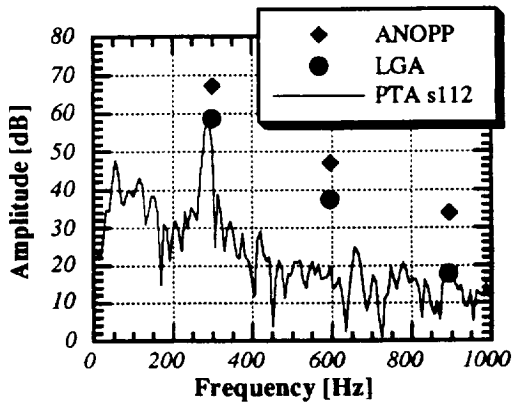

Figure 13. Far-field noise prediction of LGA compared with PTA acoustic measurements[14] and NASA's ANOPP program[13].

5. Caustics Evaluation

Technically, a caustic occurs when the ray tube area in geometrical acoustic theory goes to zero. This can either happen when multiple rays cross each other instantaneously or when a ray undergoes extensive refraction such that the velocity vector is parallel to the horizontally-stratified plane. As a result, there are primarily two types of caustics that are important to Propfan noise propagation - atmospheric caustics and homogeneous caustics. Because of their noise properties, it is important to know the location of these caustics and determine their sound intensity for annoyance considerations. A careful study of these caustics is essential in order to understand their development and to spawn efforts to redirect these caustics away from populated areas.

Atmospheric caustics

This particular form of ray focusing phenomena is an unavoidable phenomenon caused by the bending of rays due to changing atmospheric sound speed. As the rays bend gradually to become parallel to the ground plane, the linear theory of geometric acoustics leads to a diminishing ray tube area and consequently infinite pressure strength at these caustics. The occurrence of atmospheric caustics can be related to the emission angle χ in our LGA program. In an atmosphere with a constant sound speed gradient, the caustic will appear at sea-level when a ray is emitted at the emission angle χ_{caus} given by Snell's law,

$$\chi_{caus} = \mathrm{Sin}^{-1}\left[\frac{c_0}{c(R)}\right] \qquad (5.1)$$

χ_{caus} corresponds to about 61.9 degrees in LGA's calculation for the Propfan cruising at 9600 meters. Therefore any rays that are emitted with such an angle will subsequently form an atmospheric caustic. Rays that are emitted at an angle less than χ_{caus} will reach the ground plane, while those that are emitted with an angle greater than χ_{caus} will not as they will continuously be refracted back in to the upper atmosphere. Gill and Seebass[5] have looked into the acoustic outcomes at such caustics. Their predictions of caustic strength asserted that noise level will be amplified by 7 to 12 dB if an atmospheric caustic is encountered. Figure 13 shows the location of the atmospheric caustics superposed on a coarse Propfan sound carpet grid. It is apparent that the locus of the atmospheric caustics defines the outer limit of the Propfan noise carpet. Therefore, the outer limit is referred to as the atmospheric caustics-ground locus. Since all the rays arriving after an atmospheric caustic are refracted back in to the atmosphere, there cannot be any rays reaching observers beyond the outer limit . These caustics are formed by rays that have propagated over extremely long distances and have therefore experienced considerable amount of energy erosion by atmospheric effects. LGA calculations have indicated that the rays would have experienced about 47 dB attenuation by absorption and 16 dB by turbulence scattering for the fundamental frequency. These values correspond to about four times more than the attenuation due to atmospheric effects for rays in the core region. The additional dissipation of acoustic energy is more than enough to neutralize the 7 to 12 dB noise amplification predicted by Gill and Seebass at the caustic. Based on these findings, it is suffice to conclude that these atmospheric caustics are not a noise problem for the Propfan.

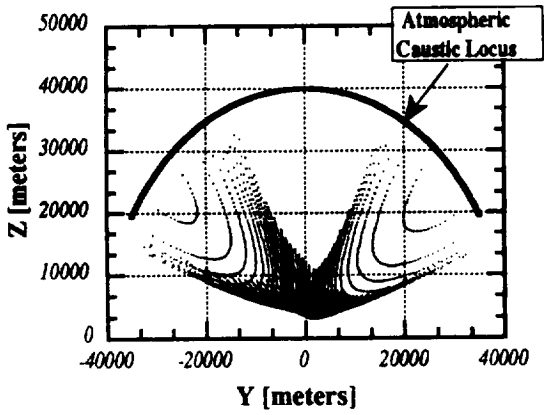

Figure 13. Location of atmospheric caustics on Propfan noise carpet.

Homogeneous caustics

Homogeneous caustics are created due to the helical motion of a supersonic propeller blade tip where two or more rays have a chance to cross each others path at the same instant. In effect, the caustics are none other than crossing wavefront created by spherically spreading signals. It has been noticed that the Mach envelopes of figure 7b correspond to the arcs observed in LGA noise carpet. The cusps are the end points of the arc which fall along the cusps caustics-ground locus and has more than two simultaneous rays arriving. The region inside the core of the noise carpet contains Mach envelopes which have two rays striking a ground observer at any instant. These Mach envelopes (cell) and cusps caustics are observed to 'sweep' across the entire plane leading to a sound field dominated by homogeneous caustics and a potential noise problem.

Myers and Wydeven[9] have provided a numerical mean to assess the acoustic amplitude at these caustics including the points along the inner limit. They accomplished the task by investigating the behavior of a distribution of supersonic singularities in helical motion in a uniform medium. Wydeven and Myers had shown that the overall near-field acoustics of the Propfan can be characterized by the Mach envelope waves generated by the supersonic portion of the blade. They have also shown that the locus of the cusps due to a single supersonic source is a hyperboloid of revolution given by,

$$x'^2 + y'^2 = \frac{z'^2}{\left\{\frac{V_h^2}{c_0^2} - 1\right\}} + \eta^2 - \frac{c_0^2}{\omega^2}\left\{\frac{V_h^2}{c_0^2} - 1\right\} \qquad (5.2)$$

where, x', y' and z' are Cartesian coordinates translating in z' direction with forward velocity, V.

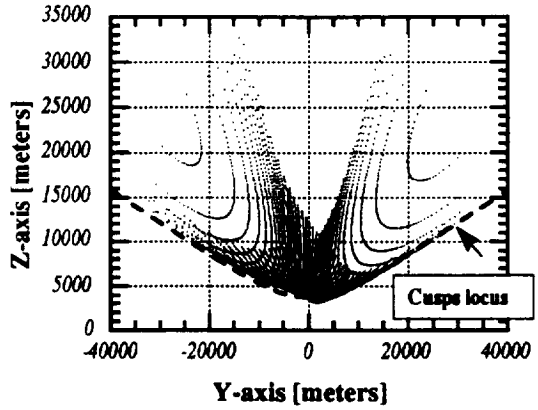

Figure 15. Location of the cusps (dashed lines) predicted by Myers et al[8] on the Propfan noise carpet.

Superposing equation (5.2) on the noise carpet, it is clear from figure 15 that the points on the cusps caustics-ground locus described by the inner limit are in fact the cusps predicted by Myers and Farassat[8]. The dash line traces the theoretical locations where the cusps reach the ground plane. It is the multiple (≥ 2) arriving rays along the cusps locus that poses the greatest annoyance problem to ground observers. LGA does an adequate job in predicting the location of these cusps, but however is not capable of predicting the acoustic noise amplitude at these points.

6. Conclusions

A survey of Propfan propagation noise is presented using geometrical acoustics theory. The far-field Propfan noise carpet consists entirely of caustics which are created by the rotational geometry of the blade tip path. Geometrical decay and atmospheric absorption are the primary factors in noise attenuation. It is necessary to account for turbulence scattering effects to obtain better noise predictions. Nonlinear wave steepening has minimal effect compared to geometrical spreading. Pressure amplifications due to atmospheric caustics are offset by dissipation incurred during acoustic propagation.

Several recommendations for Propfan noise reduction can be proposed after reviewing the various elements of Propfan noise propagation. The most obvious solution is to increase the cruise height such that a ray experiences more geometrical decay and atmospheric attenuation. A more subtle noise reducing approach uses ray bending phenomenon that prevents the rays from reaching the ground. In principle, this can be achieved by changing the rotational speed at each helix path station accordingly such that the rays are emitted at greater than χ_{caust}. Although it is probably not practical, implementation of this strategy would eliminate noise due to supersonic tip speed and caustics. Finally, it is also suggested that the acoustic energy of pure tones could be spread over a frequency regime to create weaker tones by spacing the blades unevenly.

References

1. Dunn, M. H., and Farassat, F., "State-of-the-Art of High Speed Propeller Noise Prediction - A Multidisciplinary Approach and Comparison with Measured Data," AIAA-90-3934, *AIAA 13th Aeroacoustics Conference*, Tallahassee, Florida, October 22-24, 1990.

2. Dunn, M. H., and Tarkenton, G. M., "Users Manual for the Langley High Speed Propeller Noise Prediction Program (DFP-ATP)," NASA CR NAS1-1800, 1988.

3. George, A. R., and Plotkin, K. J., "Propagation of Sonic Booms and Other Weak Nonlinear Waves Through Turbulence," *The Physics of Fluids*, 14, No. 3, pp. 548-554 (1971).

4. George, A. R., and Plotkin, K. J., "Sonic Boom Waveforms and Amplitudes in a Real Atmosphere" AIAA Journal, 7, No. 10 (1969).

5. Gill, P. M. and Seebass, A. R., "Nonlinear acoustic behavior at a caustic: an approximate analytical solution," *Prog. Astronaut. Aeronaut.*, 38, 1975, 353-386.

6. Hayes, W. D., Haefeli, R. C., and Kulsrud, H. E., "Sonic Boom Propagation in a Stratified Atmosphere with Computer Program," NASA CR-1299, April 1969.

7. Lowson, M. V. and Jupe, R. J., "Waveforms for a Supersonic Rotor," *Journal of Sound and Vibration*, 37. No. 4, pp. 475-489 (1974).

8. Myers, M. K. and Farassat, F., "Structure and Propagation of Supersonic Singularities from Helicoidal Sources," AIAA-87-2676, *AIAA 11th Aeroacoustics Conference*, Palo Alto, CA, October 19-21, 1987.

9. Myers, M. K. and Wydeven, R., "Asymptotic/Numerical Analysis of Supersonic Propeller Noise," AIAA 89-1078, *AIAA 12th Aeroacoustics Conference*, San Antonio, TX, April 10-12, 1989.

10. Pierce, A. D., *Acoustics: An Introduction to its Physical Principles and Applications*, McGraw-Hill, New York, 1981.

11. *U.S. Standard Atmosphere, 1962*, U.S. Government Printing Office, Washington, D.C., 1962

12. Whitham F.R.S., G. B., *Linear and Nonlinear Waves*, Wiley-Interscience, New York, 1974.

13. Zorumski, W. E. and Weir, D. S., "Aircraft Noise Prediction Program Theoretical Manual - Propeller Aerodynamics and Noise," NASA TM 83199 Part 3, June 1986.

14. Willshire, W., Propfan Test Assessment acoustics data, Private Communication, 1990.